Stoichiometry of altered hERG1 channel gating by small molecule activators

Wei Wu,[1,2] Frank B. Sachse,[2,3] Alison Gardner,[1,2] and Michael C. Sanguinetti[1,2]

[1]Division of Cardiovascular Medicine, Department of Internal Medicine, [2]Nora Eccles Harrison Cardiovascular Research and Training Institute, and [3]Department of Bioengineering, University of Utah, Salt Lake City, UT 84112

Voltage-gated K^+ channels are tetramers formed by coassembly of four identical or highly related subunits. All four subunits contribute to formation of the selectivity filter, the narrowest region of the channel pore which determines K^+ selective conductance. In some K^+ channels, the selectivity filter can undergo a conformational change to reduce K^+ flux by a mechanism called C-type inactivation. In human *ether-a-go-go*–related gene 1 (hERG1) K^+ channels, C-type inactivation is allosterically inhibited by ICA-105574, a substituted benzamide. PD-118057, a 2-(phenylamino) benzoic acid, alters selectivity filter gating to enhance open probability of channels. Both compounds bind to a hydrophobic pocket located between adjacent hERG1 subunits. Accordingly, a homotetrameric channel contains four identical activator binding sites. Here we determine the number of binding sites required for maximal drug effect and determine the role of subunit interactions in the modulation of hERG1 gating by these compounds. Concatenated tetramers were constructed to contain a variable number (zero to four) of wild-type and mutant hERG1 subunits, either L646E to inhibit PD-118057 binding or F557L to inhibit ICA-105574 binding. Enhancement of hERG1 channel current magnitude by PD-118057 and attenuated inactivation by ICA-105574 were mediated by cooperative subunit interactions. Maximal effects of the both compounds required the presence of all four binding sites. Understanding how hERG1 agonists allosterically modify channel gating may facilitate mechanism-based drug design of novel agents for treatment of long QT syndrome.

INTRODUCTION

Dysfunction of human *ether-a-go-go*–related gene (hERG) channels is implicated in several pathologies, including cardiac arrhythmia (Curran et al., 1995), cancer (Bianchi et al., 1998), epilepsy (Zamorano-León et al., 2012), and schizophrenia (Huffaker et al., 2009). In the human heart, hERG1 channels conduct the rapid delayed rectifier K^+ current I_{Kr} (Sanguinetti et al., 1995; Trudeau et al., 1995), a major determinant of cardiac action potential repolarization (Sanguinetti and Jurkiewicz, 1990). Reduced hERG1 function caused by mutation of *KCNH2* (Curran et al., 1995) delays ventricular repolarization, prolongs duration of the QT interval, and increases the risk of life-threatening torsades de pointes arrhythmia and ventricular fibrillation (Keating and Sanguinetti, 2001). Torsades de pointes and ventricular fibrillation can also be caused by block of hERG1 channels by a wide variety of common medications (Fenichel et al., 2004). Thus, screening of new chemical entities for hERG1 channel block is now routinely performed during an early stage of the drug development process.

The large-scale screening of compounds for hERG1 channel activity fortuitously resulted in the discovery of several hERG1 activators (Kang et al., 2005; Zhou et al., 2005; Hansen et al., 2006; Perry et al., 2009; Gerlach et al., 2010). Refinement of target selectivity and safety of these agents may eventually provide a novel therapeutic approach for treatment of arrhythmias associated with inherited or acquired long QT syndrome. Two hERG1 agonists, PD-118057 (2-(4-[2-(3,4-dichloro-phenyl)-ethyl]-phenylamino)-benzoic acid; Zhou et al., 2005) and ICA-105574 (3-nitro-*N*-(4-phenoxyphenyl) benzamide; Kang et al., 2005), have been extensively characterized and shown to differentially affect hERG1 channel gating. Hereafter we abbreviate PD-118057 as PD and ICA-105574 as ICA. PD increases single channel open probability (P_o) with a comparatively minor effect on inactivation and no effect on kinetics of activation or deactivation, single channel conductance, or gating currents (Zhou et al., 2005; Perry et al., 2009). ICA increases the magnitude of outward hERG1 currents by profound attenuation of inactivation (Gerlach et al., 2010; Garg et al., 2011). The putative binding sites for PD and ICA have been determined by a site-directed mutagenesis approach. Both compounds bind to a hydrophobic pocket located between adjacent hERG1 subunits. As voltage-gated K^+ (Kv) channels are tetrameric complexes (MacKinnon, 1991), a homotetrameric channel would be expected to contain four identical activator binding sites.

It is unknown whether one or all four of the putative hERG1 agonist–binding sites must be occupied for full activity of compounds such as PD or ICA. Moreover, it is unknown whether ligand-bound subunits act independently

Correspondence to Michael C. Sanguinetti: sanguinetti@cvrti.utah.edu

The Rockefeller University Press $30.00
J. Gen. Physiol. Vol. 143 No. 4 499–512
www.jgp.org/cgi/doi/10.1085/jgp.201311038

Supplemental material can be found at:
http://doi.org/10.1085/jgp.201311038

to enhance channel currents or whether subunit cooperativity is required. To answer these questions, we constructed concatenated hERG1 tetramers that contained a variable number (zero to four) of WT and mutant subunits with specified stoichiometry and geometry. Each mutant subunit contained a single amino acid substitution that disrupted a single PD- or ICA-binding site. Homotypic and heterotypic concatenated channels were heterologously expressed in *Xenopus laevis* oocytes, and the two-electrode voltage-clamp technique was used to characterize the effects of hERG1 agonists on channel properties. Our findings suggest that the full agonist activity of both compounds requires binding to multiple sites and involves cooperative subunit interactions.

MATERIALS AND METHODS

Construction of hERG1 concatemers

cDNAs were cloned into the pSP64 oocyte expression vector. Mutations in *KCNH2* (*HERG1*, isoform 1a; NCBI Nucleotide accession no. NM_000238) were introduced using the QuikChange site-directed mutagenesis kit (Agilent Technologies). HindIII sites were used to link two *KCNH2* monomers, and KpnI sites were used to link two *KCNH2* tandem dimers. Details of how monomers and dimers were linked together to construct fully concatenated tetramers is described in Fig. S1. Each position within the *KCNH2* tetramer was engineered to contain cDNA that encoded either a WT or a mutant subunit containing a single point mutation (L646E or F557L). All constructs were verified by DNA sequence analysis. Tetrameric *KCNH2* plasmids were linearized with EcoR1 before in vitro transcription using the mMessage mMachine SP6 kit (Ambion).

Solutions and drugs

The extracellular solution used for voltage-clamp experiments contained (mM): 98 NaCl, 2 KCl, 1 $CaCl_2$, 1 $MgCl_2$, and 5 HEPES; pH was adjusted to 7.6 with NaOH. PD and ICA (Sigma-Aldrich) were individually dissolved in DMSO to make 20-mM stock solutions. Final drug concentrations of 1–30 µM (the limit of solubility) were obtained by dilution of the stock solution with extracellular solution immediately before use for each experiment.

Isolation and voltage clamp of *Xenopus* oocytes

Procedures used for the surgical removal of ovarian lobes from *Xenopus* and isolation of oocytes were approved by the University of Utah Institutional Animal Care and Use Committee and performed as described previously (Abbruzzese et al., 2010). Single oocytes were injected with 10 ng cRNA encoding single hERG1 subunits and studied 1–3 d later. hERG1 tandem dimers and concatenated tetramers expressed poorly, and therefore, oocytes were injected with 50 ng cRNA and studied 4–8 d later. Ionic currents were recorded using agarose-cushion microelectrodes (Schreibmayer et al., 1994) and standard two-electrode voltage-clamp techniques (Goldin, 1991; Stühmer, 1992). A GeneClamp 500 amplifier, Digidata 1322A data acquisition system, and pCLAMP 8.2 software (Molecular Devices) were used to produce command voltages and to record current and voltage signals.

Data analysis

Digitized data were analyzed offline with pCLAMP8 and ORIGIN 8.5 (OriginLab) software. To determine the conductance-voltage relationship, 4-s pulses were applied to test potentials (V_t) that ranged from −70 to 50 mV. Normalized conductance (G/G_{max}) defined as the amplitude of tail currents (I_{tail}) measured at −70 mV normalized to their maximum value ($I_{tail\text{-}max}$) was plotted as a function of V_t. The relationship was fitted with a Boltzmann function to determine the half-point ($V_{0.5act}$) and the equivalent charge (z) for channel activation:

$$\frac{I_{tail}}{I_{tail\text{-}max}} = \frac{G}{G_{max}} = \frac{1}{1+e^{-zF(V_t - V_{0.5act})/RT}},$$

where F is the Faraday constant, R is the gas constant, and T is the absolute temperature. To estimate the voltage dependence of C-type inactivation, an initial 1-s pulse to 40 mV was followed by a 5-s pulse to a variable return potential (V_{ret}) that ranged from 30 to −140 mV. For all channel types, $I_{tail}/(V_{ret} - E_{rev})$ was plotted as a function of V_{ret}, and the relationship was fitted with a Boltzmann function to estimate $V_{0.5}$ for inactivation ($V_{0.5inact}$) and z.

The fold increase (*FI*) in hERG1 current (either $I_{tail\text{-}max}$ or the magnitude of test currents, I_{test}) induced by drug was plotted as a function of [PD] or [ICA], and the resulting relationship was fitted with a modified logistic equation:

$$FI = FI_{max} + \frac{1 - FI_{max}}{1 + \left([drug]/EC_{50}\right)^{n_H}},$$

where EC_{50} is the concentration of compound that produced a half-maximal effect, and n_H is the Hill coefficient. Data are presented as mean ± SEM (n = number of individual oocytes). Where appropriate, data were analyzed with a two-way ANOVA or paired Student's t test; $P < 0.05$ was considered significant. For some plots, the goodness of fit was evaluated by the coefficient of determination (adjusted R^2).

Modeling of hERG1 channels

Markov models were developed to reconstruct measured currents of concatenated WT tetramers in the presence and absence of 30 µM PD or ICA. The models comprised five closed, one open, and one inactivated state (see Fig. 2 A). Coupling of states was described by transition rates. The transition rates α_{CO} and β_{CO} had constant values. Otherwise, forward rates α and backward rates β were defined as dependent on the transmembrane voltage V_m:

$$\alpha = \alpha_o e^{z_\alpha V_m F/RT}$$
$$\beta = \beta_o e^{-z_\beta V_m F/RT},$$

with the rates α_0 and β_0 at 0 mV, the charges z_α and z_β, and the temperature T (293°K). Current I_{hERG} conducted by concatenated tetramers was described as

$$I_{hERG} = OG_{hERG}\sqrt{\frac{[K^+]_O}{4mM}}(V_m - E_K),$$

with the conductance G_{hERG}, the extracellular potassium concentration $[K^+]_o$ in mM, the reversal voltage E_K, and open state probability O (Iyer et al., 2004).

Parameters of the Markov models were determined using a previously developed stochastic multiscale fitting routine (Abbruzzese et al., 2010). In short, the fitting applied feature vectors were extracted from experimental data f_e and compared with feature vectors of simulation data f_m using a fit error function E, and E was iteratively minimized. Features were extracted from measured and simulated I_{hERG} at different voltages and

included maxima and parameters from exponential fits. The function E was defined as

$$E = \sqrt{\sum_{i=1\ldots n} \left(\frac{\left\| f_{m,i} - f_{e,i} \right\|_2}{\left\| f_{e,i} \right\|_2} \right)^2 + \left(1 - \mathrm{Max} \sum_j C_j \right)^2 + \left(O_{\mathrm{Max}} - \mathrm{Max}\, O \right)^2 + \left(1 - \mathrm{Max}\left(C_4 + O + I \right) \right)^2},$$

with the number of features n, the Euclidean norm $\|\ldots\|_2$, the maximal closed state probability at the end of the prepulse $\mathrm{Max}\sum_j C_j$, the maximal open state probability O during the test pulses, a predefined maximal open state probability O_{Max}, the maximal probability of the fourth closed state C_4 during the test pulses, and the maximal probability of the inactivated state I during the test pulses. O_{Max} was set to 0.1 in parameter optimization of the control model. O_{Max} for PD and ICA models was scaled by the ratio of maximal $I_{test\text{-}end}$ after activator application and maximal $I_{test\text{-}end}$ under control conditions. Max O was calculated for each parameter set during stochastic optimization aimed at minimizing the difference between Max O and O_{Max}. Modeling and parameter fitting software was implemented in Matlab R2011b (The Mathworks Inc.) and the Matlab Parallel Computing Toolbox. Simulations were performed with variable order method for solution of ordinary differential equations based on numerical differentiation formulas (Matlab function: ode15s) using an initial time step Δt of 1 ms. The initial value for the state C_0 was 1. Initial values for all other states were 0.

Online supplemental material

Fig. S1 shows schematic plasmid maps for hERG1 monomers, tandem dimers, and concatenated tetramers. Tables S1 and S2 list the initial and calculated values of rate constant parameters for modeling effects of PD and ICA, respectively. Tables S3 and S4 list the features for fitting and fit errors for the PD and ICA models, respectively. Online supplemental material is available at http://www.jgp.org/cgi/content/full/jgp.201311038/DC1.

RESULTS

Concatenated homotetrameric WT hERG1 channels have normal gating and pharmacology

Ionic currents in *Xenopus* oocytes expressing single WT subunits or concatenated WT homotetramers (WT_4) measured by two-microelectrode voltage clamp had similar kinetics (Fig. 1 A). The voltage dependence of activation and C-type inactivation for these channels was nearly identical (Fig. 1 B), but as reported previously for concatenated Shaker K^+ channels (Tytgat and Hess, 1992), the rate of deactivation of tail currents was slightly faster for WT_4 compared with WT hERG1 channels (Fig. 1 C). The effects of two hERG1 activators on the two channel types were also examined. At a concentration of 10 µM, PD

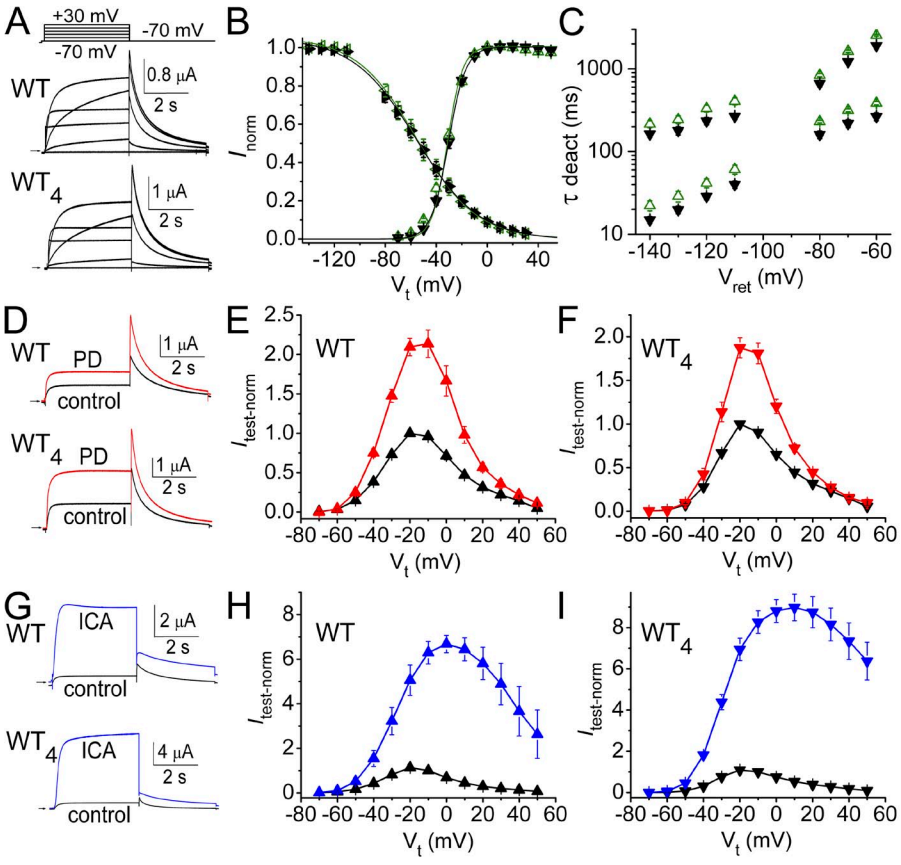

Figure 1. Concatenated tetrameric hERG1 (WT_4) channels have similar biophysical and pharmacological properties as channels formed by coassembly of single WT hERG1 subunits. (A) Representative WT and WT_4 hERG1 channel currents recorded at the indicated V_t (−70 to 30 mV stepped in 20-mV increments). (B) The voltage dependence of WT channel gating (upright green triangles, activation; sideways green triangles, C-type inactivation) is similar to WT_4 channels (upside-down black triangles, activation [$n = 6$]; sideways black triangles, C-type inactivation [$n = 8$]). Data were fitted to Boltzmann function (smooth curves) to determine $V_{0.5act}$ and z values (presented in Table 1). (C) Time constants (τ deact) for fast and slow components of current deactivation for WT (green triangles, $n = 10$) and WT_4 (black triangles, $n = 11$) channels at the indicated return potential (V_{ret}). (D) Effect of 10 µM PD on WT and WT_4 hERG1 channel currents elicited by 4-s step to 0 mV. I_{tail} was measured at −70 mV. (E and F) I_{test}-V_t relationships in the absence (black triangles) and presence of 10 µM PD (red triangles) for oocytes injected with cRNA encoding single WT subunits (E, $n = 10$) or WT_4 channels (F, $n = 7$). Currents were normalized to peak I_{test} (at −20 mV) measured under control conditions. (G) Effect of 10 µM ICA on currents for WT and WT_4 channels. (H and I) I_{test}-V_t relationships in the absence (black triangles) and presence of 10 µM ICA (blue triangles) for oocytes injected with cRNA encoding single WT subunits (H, $n = 5$) or WT_4 channels (I, $n = 10$). Data are expressed as mean ± SEM (n = number of oocytes).

increased I_{test} measured at the end of 4-s pulses about twofold with no change in kinetics for both WT and WT_4 hERG1 channels (Fig. 1, D–F). ICA at 10 µM induced a much larger increase in I_{test} magnitude and slowed current deactivation in both WT and WT_4 hERG1 channels (Fig. 1 G). Consistent with the known inhibitory effects of ICA on inactivation, enhancement of current was voltage dependent (e.g., 4- and 20-fold increase at −30 mV and 20 mV, respectively), resulting in reduced rectification of the isochronal (4 s) I_{test}-V_t relationships (Fig. 1, H and I). Thus, the biophysical and pharmacological properties of hERG1 channels were similar whether formed by cellular coassembly of single subunits or preformed by concatenation of four identical protomers.

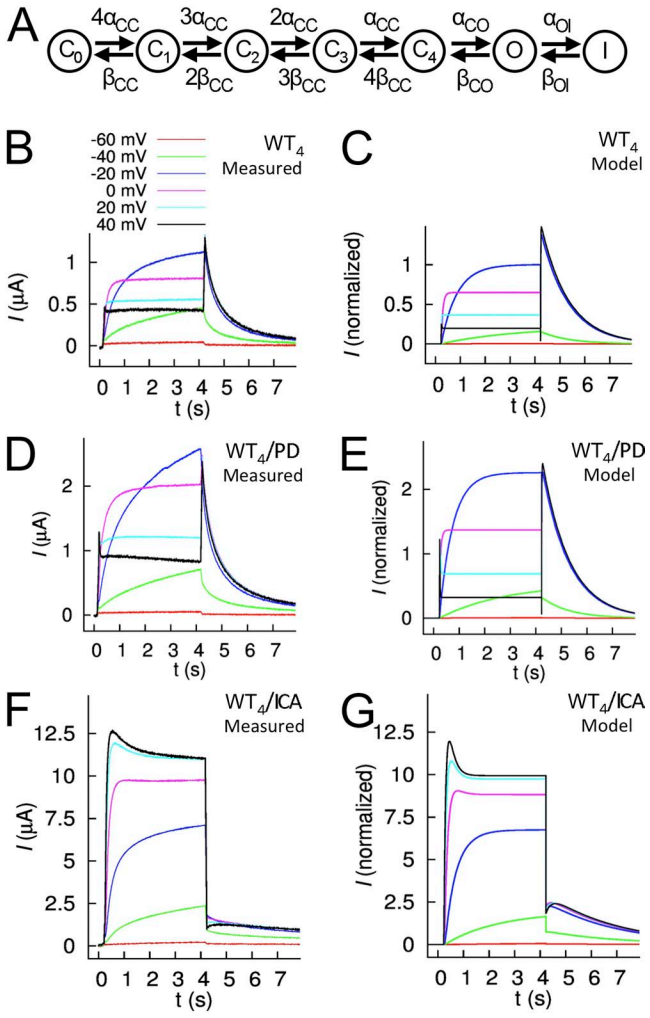

Figure 2. Markov modeling of hERG1 tetrameric channel currents modified by drugs PD and ICA. (A) The model comprises seven states (C_0,…,C_4, closed states; O, open state; I, inactivated state) coupled with the indicated rate coefficients. (B) Averaged currents (n = 4) from oocytes expressing WT_4 tetramers under control conditions in response to voltage steps to the indicated V_t. (C) Simulated currents for WT_4 tetramers under control conditions. (D and E) Averaged currents measured from the same oocytes as in B, after application of 30 µM PD (D), and corresponding simulated currents (E). (F and G) Averaged currents (n = 6) measured after application of 30 µM ICA (F) and corresponding simulated currents (G). Currents shown in B, D, and F were not leak subtracted.

Markov models of hERG1 channel gating

Markov models were developed to quantitatively describe the changes in gating of WT_4 channels induced by 30 µM PD or ICA. The models comprised five closed states, one open, and one inactivated state (Fig. 2 A). Rate coefficients of the models were determined by a previously developed stochastic optimization approach (Abbruzzese et al., 2010) using features extracted from averaged current traces. The WT_4 model reconstructs major features of measured currents (Fig. 2, B and C), in particular, voltage-dependent activation, rapid recovery from inactivation, and slow deactivation. Fig. 2 (D and E) presents averaged measured current traces of concatenated WT_4 tetramers after application of 30 µM PD together with simulated currents. To simulate the effects of PD, several rate coefficients were altered, including reduction of α_{OI} by 76% and β_{OI} by 46% (Table S1). Fig. 2 (F and G) presents averaged measured current traces of concatenated WT_4 tetramers after application of 30 µM ICA together with simulated currents. To simulate the effects of ICA, the main changes were a reduction of α_{OI} to 0.1% and β_{OI} to 6.7% (Table S2). Tables S3 and S4 list the features for fitting and fit errors for the PD and ICA models. Alterations in multiple gating parameters predicted by these models precluded simple analysis of drug effects on the heterotypic channels.

Cooperative subunit interactions mediate the agonist activity of PD

Using a combined approach of functional analysis of mutant channels and molecular modeling, the putative binding site for PD was previously shown to be localized to a hydrophobic pocket between the S5 and S6 segments of adjacent hERG1 subunits (Perry et al., 2009). A point mutation in S6 (L646E) eliminated activity of PD, and molecular modeling predicted this was caused by steric interference with ligand binding (Perry et al., 2009). A homotetrameric hERG1 channel has four identical intersubunit PD binding sites, but it is unknown whether drug binding to one or multiple sites is required to enhance channel currents. Six concatenated tetramers containing a variable number (zero to four) of L646E subunits were constructed (Fig. S1). These channels are designated here as LE_n/WT_{4-n}, where LE represents L646E mutant subunits, WT represents WT hERG1 subunits, and the subscript n indicates the number of L646E subunits in a concatenated tetramer. Included in the constructs were two tandem dimers in which WT subunits were located in an adjacent (LE_2/WT_2) or diagonal ($LE_1/WT_1/LE_1/WT_1$) orientation and two tetramers containing a single L646E subunit in either the first (LE_1/WT_3) or last (WT_3/LE_1) position.

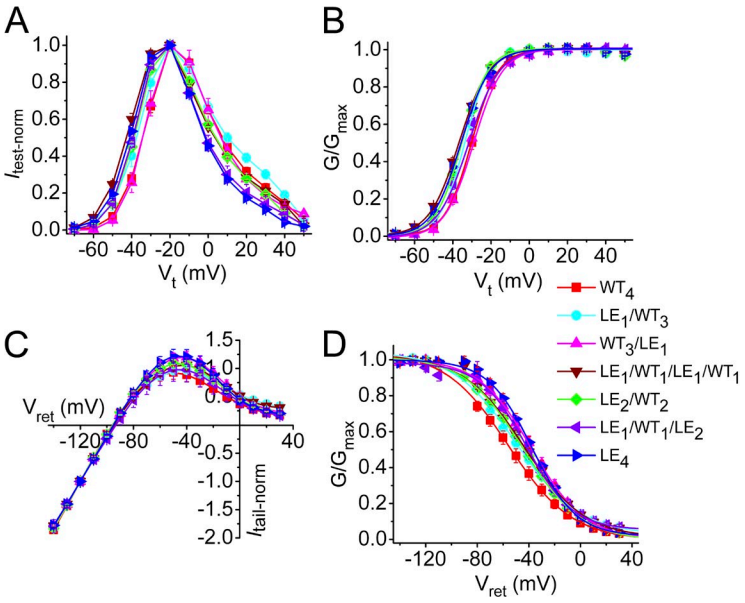

Figure 3. Biophysical properties of concatenated LE_n/WT_{4-n} tetrameric hERG1 channels. (A) I_{test}-V_t relationships. (B) Voltage dependence of activation. (C) Fully activated I_{tail}-V_{ret} relationships. (D) Voltage dependence of inactivation. Legend refers to all panels. Data are expressed as mean ± SEM (n = 5–12; values for $V_{0.5}$ and z for activation and inactivation are presented in Table 1; n = number of oocytes).

Fig. 3 (A–D) illustrates that the biophysical properties of channels containing zero to four L646E mutant subunits, including I-V relationships and voltage dependence of gating, were only slightly altered compared with WT_4 channels. Table 1 summarizes the $V_{0.5}$ and z values for the activation and inactivation relationships for these channels. Representative current traces recorded during a 4-s pulse to 0 mV in the absence and presence of 10 µM PD are illustrated for five tetramers in Fig. 4 A. The most prominent effect of the compound was an increase in the magnitude of I_{tail} measured upon repolarization to −70 mV. The voltage dependence of homotypic or heterotypic channel activation, determined by fitting the I_{tail}-V_t relationship to a Boltzmann function, was not altered by 10 µM PD (Fig. 4 B and Table 1), but $I_{tail-max}$ was increased as the number of WT subunits was increased from one to four (Fig. 4 B). C-type inactivation is modestly inhibited by PD (Perry et al., 2009). However, based on an analysis of I_{tail}, most of the agonist effects of PD can be attributed

TABLE 1

Summary of effects of PD on the voltage dependence of activation and inactivation for hERG1 monomers (WT) and tetramers containing zero to four L646E (LE) subunits

Channel type	Control		10 µM PD		n
	$V_{0.5}$	z	$V_{0.5}$	z	
	mV		*mV*		
$V_{0.5act}$					
WT hERG1	−29.8 ± 0.8	3.41 ± 0.09	−29.2 ± 14	3.07 ± 0.34	6
WT_4	−29.1 ± 0.9	3.45 ± 0.33	−26.7 ± 1.0	3.07 ± 0.30	8
LE_1/WT_3	−32.1 ± 1.3	4.13 ± 0.14	−30.1 ± 1.6	4.20 ± 0.07	11
WT_3/LE_1	−29.1 ± 1.5	3.36 ± 0.21	−27.1 ± 1.29	3.44 ± 0.16	4
$LE_1/WT_1/LE_1/WT_1$	−36.7 ± 0.5	3.23 ± 0.08	−32.7 ± 0.8	3.45 ± 0.19	6
LE_2/WT_2	−35.4 ± 0.8	3.88 ± 0.12	−31.3 ± 1.0	3.94 ± 0.12	12
$LE_1/WT_1/LE_2$	−33.5 ± 1.6	3.41 ± 0.18	−30.3 ± 1.4	3.55 ± 0.15	6
LE_4	−36.5 ± 1.0	3.55 ± 0.20	−32.6 ± 1.2	3.55 ± 0.25	9
$V_{0.5inact}$					
WT hERG1	−55.8 ± 3.7	1.19 ± 0.02	−34.7 ± 4.2	1.19 ± 0.09	5
WT_4	−55.7 ± 0.7	1.10 ± 0.02	−39.4 ± 4.6	1.26 ± 0.17	4
LE_1/WT_3	−48.5 ± 2.7	1.02 ± 0.05	−44.6 ± 2.7	1.24 ± 0.10	8
WT_3/LE_1	−37.4 ± 3.0	1.23 ± 0.02	−33.5 ± 3.7	1.44 ± 0.19	4
$LE_1/WT_1/LE_1/WT_1$	−42.6 ± 3.6	1.08 ± 0.05	−43.3 ± 3.4	1.22 ± 0.07	5
LE_2/WT_2	−45.7 ± 1.9	1.07 ± 0.03	−45.5 ± 2.8	1.19 ± 0.08	7
$LE_1/WT_1/LE_2$	−44.3 ± 5.5	1.27 ± 0.08	−47.7 ± 4.0	1.31 ± 0.08	4
LE_4	−41.4 ± 1.6	1.49 ± 0.04	−43.6 ± 2.2	1.52 ± 0.05	6

Data are expressed as mean ± SEM (n = number of oocytes).

to its effect on P_o. Tail currents elicited at a variable return potential (V_{ret}) after a 1-s pulse to 40 mV (Fig. 4 C) were used to construct a fully activated I_{tail}-V_{ret} relationship (Fig. 4 D). The increase in I_{tail} at −140 mV (68%), where recovery from inactivation is complete, was nearly equivalent to the increase in I_{tail} at −70 mV (81%), where recovery from inactivation is ∼70% complete. Therefore, $I_{tail\text{-}max}$ at −70 mV can be used to approximate changes in P_o.

The fold increase in $I_{tail\text{-}max}$ by PD was concentration dependent for WT_4 and the heterotypic tetramers (Fig. 4 E); however, there was no significant correlation between the number of WT subunits present in a concatemer and the EC_{50} or n_H for PD (Fig. 5). This finding suggests that ligand binding is not cooperative. Extrapolation of the concentration-response relationship for WT_4 channels (Fig. 4 E) indicates that PD is predicted to increase $I_{tail\text{-}max}$ by a maximum of 1.9-fold, perhaps limited by a saturating effect on the channel open probability P_o. The maximum P_o of WT hERG1 has not been determined because at positive potentials where channels are maximally activated they are also highly inactivated. The P_o of inactivation-deficient S631A mutant channels is ∼0.5 at potentials between 40 and 80 mV (Zou et al., 1998). Assuming a maximum P_o of 0.5 for WT_4 channels in the absence of drug, we estimated P_o for each tetrameric channel from the maximum fold increase in $I_{tail\text{-}max}$ determined from extrapolation of the [PD]-response relationships as shown in Fig. 4 E. Estimates of the equilibrium constant K_{eq} ($P_o/(1 - P_o)$) were then used to calculate the free energy change associated with channel activation: $\Delta G = -RTlnK_{eq}$. If subunits acted completely independently of one another, where a conformational change in any single PD-bound WT subunit was sufficient to achieve maximal agonist activity of the compound, then ΔG for all of the heterotypic channels would be predicted to be the same as WT_4

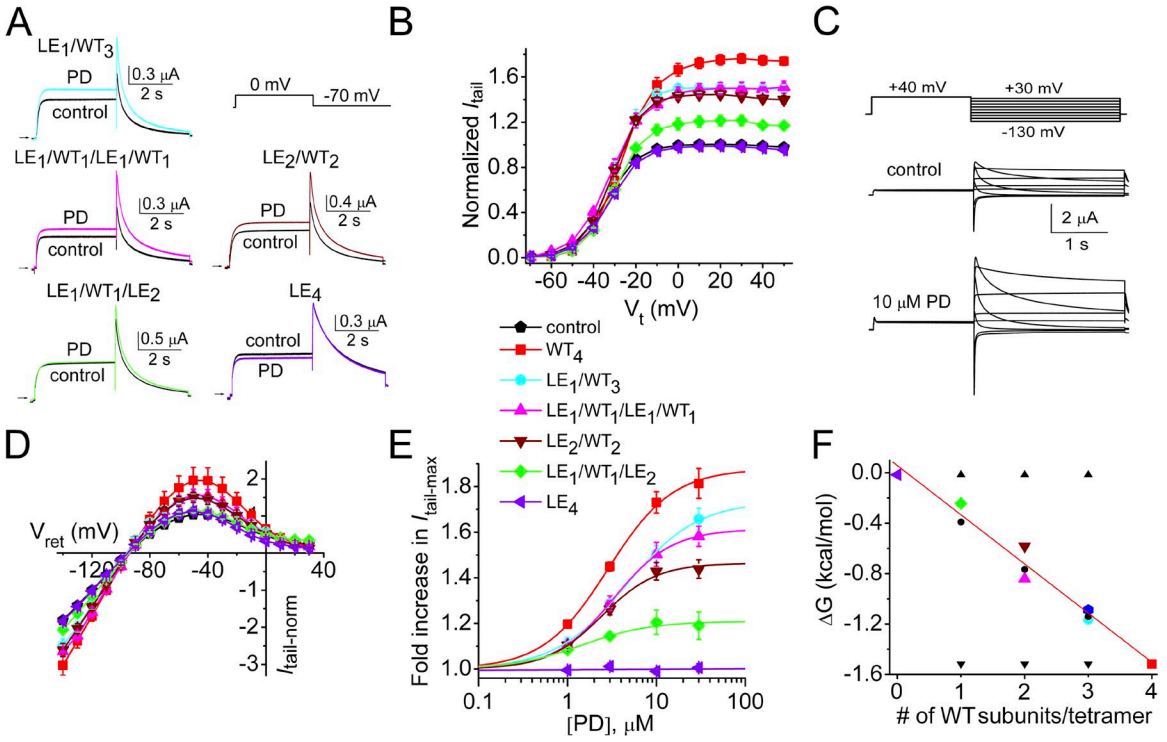

Figure 4. PD-induced enhancement of hERG1 current indicates cooperative subunit interactions. (A) Representative current traces recorded at 0 mV for concatenated tetramers containing zero to three WT subunits together with one to four L646E subunits, before and after 10 μM PD. (B) Effect of 10 μM PD on voltage dependence of channel activation. I_{tail} was measured at −70 mV after pulses to the indicated V_t and normalized to $I_{tail\text{-}max}$ under control conditions for each channel type (n = 7–15). The symbol legend between B and E refers to data plotted in B and D–F. Control I_{tail}-V_t relationship (black pentagons) overlaps data for LE_4 channels and represents the mean of all channel types. The $V_{0.5act}$ and z values obtained from fitting I_{tail}-V_t relationships to a Boltzmann function (smooth curves) before and after 10 μM PD are presented in Table 1. (C) Pulse protocol (top) used to measure fully activated I_{tail}-V_{ret} relationship and representative currents for WT_4 channels under control conditions and after 10 μM PD as indicated. (D) Effect of 10 μM PD on I_{tail}-V_{ret} relationships (n = 4–9) normalized to I_{tail} at −120 mV under control conditions for LE_n/WT_{4-n} tetramers (n = 0–4). (E) [PD]-response relationships for fold increase in $I_{tail\text{-}max}$ at −70 mV for different tetramers according to symbol legend shown between B and E. Data were fitted with a logistic equation to determine EC_{50} values and Hill coefficient, n_H (see Fig. 5). (F) Plot of ΔG versus number of WT subunits contained in a concatenated tetramer. ΔG was equal to $-RTlnK_{eq}$, where K_{eq} was defined as $P_o/(1 - P_o)$ at maximal effect of PD and assuming maximum P_o in the absence of drug to be 0.5. Linear regression analysis was used to fit calculated data (colored symbols; solid line: $y = -0.39x + 0.058$; $R^2 = 0.96$) and the relationships predicted for independent subunit transitions (▼) and cooperative subunit interactions, models 1 (▲) and 2 (●). Data are expressed as mean ± SEM (n = number of oocytes).

channels (Fig. 4 F, ▼). This model of independence is exemplified by N-type inactivation of Kv1 channels, where any one and only one N-terminal ball peptide is sufficient to induce inactivation (MacKinnon et al., 1993), and by the independent outward movement of S4 segments in response to membrane depolarization. As described in a previous study of the conformational changes that lead to activation gate opening in Shaker K^+ channels (Zandany et al., 2008), we considered two mechanistic models of subunit cooperativity. The first model is analogous to the Monod-Wyman-Changeux (Monod et al., 1965) allosteric model of ligand binding to multisubunit proteins. This model is exemplified by the final concerted step of Kv channel activation where a simultaneous conformational change in all four subunits leads to channel opening (Sigworth, 1994; Zagotta et al., 1994), as directly demonstrated using concatenated heterotetrameric Shaker K^+ channels composed of WT and mutant subunits harboring a mutation that disrupts function of the S6 glycine hinge (Zandany et al., 2008). If fully concerted, all-or-none cooperation between subunits underlies the agonist activity of PD, then the ΔG for all the heteromeric channels would be predicted to be the same as LE_4 channels (Fig. 4 F, ▲). The second model of cooperativity assumes an equal energetic contribution from each subunit to the tetrameric channel function. In this model, the predicted net free energy of a tetramer (ΔG) would be the sum of the individual values contributed by each of the WT and mutant LE subunits as follows:

$$\Delta G_{het} = \frac{n\Delta G_{WT4}}{4} + \frac{(4-n)\Delta G_{LE4}}{4},$$

where n equals the number of WT subunits in a tetramer and ΔG_{WT4} and ΔG_{LE4} are the free energy values calculated for WT_4 and LE_4 homotypic tetramers, respectively. This model of cooperativity (Fig. 4 F, ●) describes the subunit interactions that underlie the steady-state voltage dependence of activation (Hurst et al., 1992; Smith-Maxwell et al., 1998) and slow C-type inactivation (Ogielska et al., 1995; Panyi et al., 1995) in Kv channels.

The experimentally determined values of ΔG ($-RTlnK_{eq}$) were plotted as a function of the number of WT subunits in a concatenated tetramer in Fig. 4 F. The data closely match the ΔG values predicted for cooperativity model 2. Thus, PD-bound subunits contribute equally to the enhancement of currents conducted by hERG1 tetramers.

It is notable that $LE_1/WT_1/LE_1/WT_1$ channels had a greater response to PD than did the LE_2/WT_2 channels. The positioning of a mutant subunit within concatemers can affect the biophysical properties of K^+ channels (McCormack et al., 1992), and perhaps the pharmacological responses to drugs. To examine this possibility in more detail, we determined whether the biophysical properties or response to PD of WT_3/LE_1 channels differed from LE_1/WT_3 channels. These channels did not appreciably differ with respect to kinetics (Fig. 6 A), voltage dependence

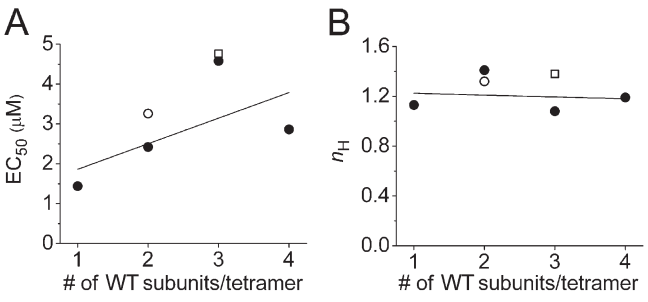

Figure 5. The concentration response relationship for PD-induced increase in I_{tail} is not dependent on the number of WT subunits in a concatenated tetramer. (A) Plot of EC_{50} as a function of the number of WT subunits in a tetramer. Line represents linear fit to data: y = 0.64x + 1.22 (adjusted R^2 = 0.099). (B) Plot of n_H as a function of number of WT subunits in a tetramer. Line represents linear fit to data: y = −0.015x + 1.24 (adjusted R^2 = −0.473). In both panels, the open circle represents $LE_1/WT_1/LE_1/WT_1$ channels; the open square represents WT_3/LE_1 channels.

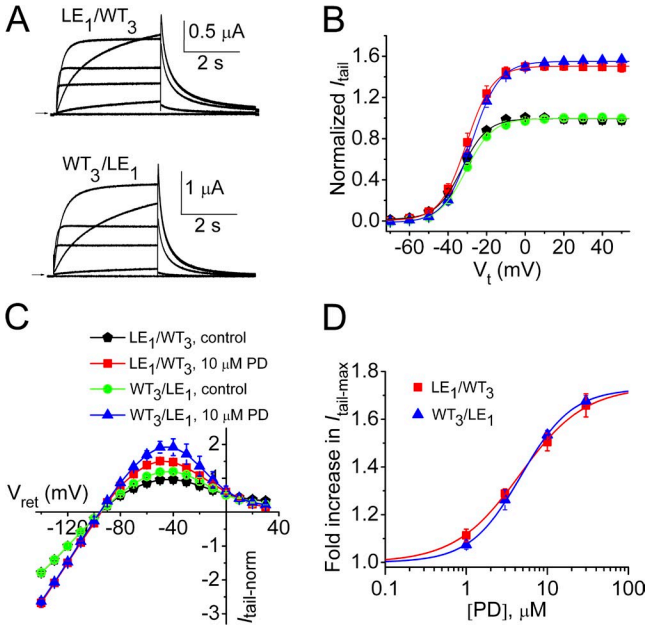

Figure 6. Positioning of a single LE mutant subunit in a concatenated hERG1 tetramer does not affect biophysical properties or response to PD. (A) Representative current traces for LE_1/WT_3 and WT_3/LE_1 hERG1 channels. Pulses were applied to V_t of −70 to 30 mV in 20-mV increments. V_h was −80 mV and V_{ret} was −70 mV. (B) Normalized I_{tail}-V_t relationships before and after 10 μM PD. Symbol legend is the same as for C. For LE_1/WT_3 hERG1 channels: $V_{0.5act}$ = −32.1 ± 1.3 mV, z = 4.13 ± 0.14 mV (control); $V_{0.5act}$ = −30.1 ± 1.6 mV, z = 4.20 ± 0.07 mV (PD; n = 11). For WT_3/LE_1 hERG1 channels: $V_{0.5act}$ = −29.1 ± 1.5 mV, z = 3.36 ± 0.21 mV (control); $V_{0.5act}$ = −27.1 ± 1.3 mV, z = 3.44 ± 0.16 mV (PD; n = 4). (C) Normalized fully activated I_{tail}-V_{ret} relationships determined before and after 10 μM PD. (D) [PD]-response relationships for LE_1/WT_3 hERG1 channels (EC_{50} = 4.6 μM, n_H = 1.1; n = 6–9) and WT_3/LE_1 hERG channels (EC_{50} = 4.8 μM, n_H = 1.4; n = 4). Data are expressed as mean ± SEM (n = number of oocytes).

of activation (Fig. 6 B), shape of the fully activated I-V relationship (Fig. 6 C), or response to PD (Fig. 6 D). Thus, unlike channels with two WT and two mutant subunits, placing a single L646E subunit in the first or fourth position of an hERG1 tetramer did not affect the biophysical properties or response to PD. A full test of the importance of mutant subunit positioning and confirmation of sequential cooperativity (Zandany et al., 2008) would require examination of all possible heteromeric tetramers.

Cooperative subunit interactions mediate attenuation of C-type inactivation by ICA

The same concatenation strategy used to characterize PD was used to study ICA, a compound which enhances hERG1 current by strongly inhibiting channel inactivation (Gerlach et al., 2010). WT subunits were linked to a variable number of subunits containing the point mutation F557L, which prevents ICA binding (Garg et al., 2011). Representative current traces recorded during 4-s test pulses and their corresponding I_{test}-V_t relationships for the different concatemers are shown in Fig. 7 (A and B). Compared with WT_4 channels, the presence of F557L mutant subunits in a concatenated tetramer induced a faster rate of current deactivation (Fig. 7 A) and produced a 5- to 14-mV shift in the voltage dependence of activation (Fig. 7 C and Table 2). In addition, for tetramers with F557L subunits, inward rectification of the fully activated I_{tail}-V_t relationship was accentuated (Fig. 7 D), and the voltage dependence of inactivation was shifted to more negative potentials (Fig. 7 E and Table 2), similar to channels formed by natural coassembly of F557L monomers (Perry et al., 2007). Thus, unlike the L646E mutation used to disrupt binding of PD, the F557L mutation altered the biophysical properties of hERG1 tetramers.

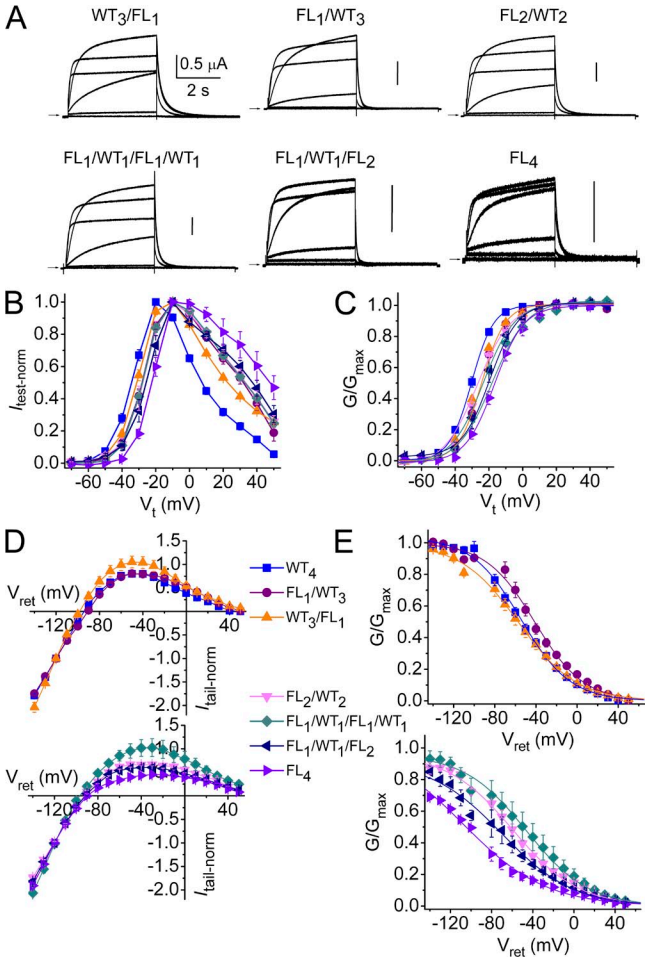

Figure 7. Biophysical properties of concatenated FL_n/WT_{4-n} tetrameric hERG1 channels. (A) Representative current traces for concatenated tetramers containing zero to three WT subunits together with one to four F557L subunits. Pulses were applied to V_t of −70 to 30 mV in 20-mV increments. V_h was −80 mV and V_{ret} was −70 mV. (B) I_{test}-V_t relationships for FL_n/WT_{4-n} tetrameric hERG1 channels. (C) Voltage dependence of activation. (D) Fully activated I_{tail}-V_{ret} relationships. (E) Voltage dependence of inactivation. The symbol legend refers to B–E. Data are expressed as mean ± SEM (n = 3–12). Values for $V_{0.5}$ and z for activation and inactivation are presented in Table S2.

We next determined the effects of ICA on FL_n/WT_{4-n} tetrameric channels. The increase in current at a V_t of 20 mV was ∼13-fold greater for WT_4 channels compared with $FL_1/WT_1/FL_2$ channels; however, the EC_{50} and n_H values were similar (Fig. 8 A). Representative current traces recorded during 4-s pulses to 0 mV in the absence and presence of 10 µM ICA are illustrated for several tetramers in Fig. 9 A. The I_{test}-V_t relationships illustrates that the effect of 30 µM ICA was enhanced at positive test potentials and by increasing the number of WT subunits (i.e., the number of functional ICA binding sites) in a tetramer (Fig. 9 B). Increasing the number of available binding sites per channel from zero (FL_4) to one ($FL_1/WT_1/FL_2$) to two ($FL_1/WT_1/FL_1/WT_1$) caused a simple additive increase in the response to 30 µM ICA, whereas addition of a third (FL_1/WT_3) and a fourth (WT_4) binding site resulted in a greater than additive effect for test potentials ranging from 0 to 40 mV (Fig. 8 B). hERG1 channels are fully activated at 20 mV. Therefore, I_{test} measured at 20 mV was used to compare the efficacy (maximal effect) of ICA for the various tetramers. The increase in I_{test} at 20 mV varied as a logarithmic function of the number of WT subunits contained in a tetramer (Fig. 9 C). Opposite to PD, channels with adjacent positioning of WT subunits (FL_2/WT_2) were increased by ICA more than channels with diagonally oriented WT subunits ($FL_1/WT_1/FL_1/WT_1$; Fig. 9, B and C).

The effect of ICA on the voltage dependence of inactivation as a function of the number of WT subunits in a tetramer was determined. The effect of 30 µM ICA on fully activated I_{tail}-V_{ret} relationships for FL_1/WT_3 and $FL_1/WT_1/FL_2$ channels are compared in Fig. 9 D. ICA had only minor effects on the I_{tail}-V_{ret} relationship for $FL_1/WT_1/FL_2$ channels but markedly reduced inward

rectification of FL_1/WT_3 channel currents. The effects of 30 µM ICA on the voltage dependence of inactivation of these two channel types are compared in Fig. 9 E. ICA caused a large positive shift in $V_{0.5inact}$ (70 ± 3 mV; n = 4) of this relationship for FL_1/WT_3 channels but only a small shift in $V_{0.5inact}$ (6.6 ± 1.6 mV; n = 4) for $FL_1/WT_1/FL_2$ channels. The effect of ICA on $V_{0.5inact}$ and z for all the concatenated tetramers are presented in Table 2. We suspected that the increase in I_{tail} at potentials negative to the reversal potential observed for FL_1/WT_3 channels (Fig. 9 D) and WT_4 channels (not depicted) resulted from an increased electrochemical gradient caused by extracellular K^+ accumulation associated with large outward currents that occur during the prepulse to 80 mV. To test for this possibility, we determined the effect of 30 µM ICA on the I_{tail}-V_{ret} relationship for WT_4 channels using a bath solution containing 20 mM KCl to greatly reduce the effect of extracellular K^+ accumulation caused by pulsing to 80 mV. Under these conditions, ICA did not cause an increase in I_{tail} at potentials more negative than −100 mV (Fig. 9 F), indicating that the increase in currents results from reduced inactivation and not an increase in maximum P_o of channels.

The $V_{0.5inact}$ and z values determined from inactivation curves were used to estimate the free energy change associated with channel inactivation (ΔG):

$$\Delta G = z \cdot F \cdot V_{0.5inact}.$$

ICA-induced perturbations in ΔG (ΔΔG) were calculated for each concatenated tetramer as

$$\Delta\Delta G = \left|\Delta G_{ICA} - \Delta G_{con}\right|,$$

where ΔG_{con} equals $zFV_{0.5inact}$ before drug, and ΔG_{ICA} equals $zFV_{0.5inact}$ determined in the presence of 30 µM ICA. If each ICA-bound subunit contributes equally to disruption of inactivation (model 2), then the predicted change in free energy (ΔΔG) of a heteromeric tetramer would be the sum of the individual ΔΔG values contributed by each of the WT and F557L subunits in a tetramer as follows:

$$\Delta\Delta G = \frac{n\Delta\Delta G_{WT4}}{4} + \frac{(4-n)\Delta\Delta G_{FL4}}{4}.$$

For this model, ΔΔG would be predicted to be a linear function of the number of WT subunits in a concatenated tetramer. Fully concerted cooperativity (model 1) predicts that a single ICA-bound WT subunit would disrupt inactivation to the same extent as channels containing two, three, or four WT subunits per tetramer. In Fig. 9 G, the experimentally determined ΔΔG values are plotted as a function of the number of WT subunits contained in a tetramer. The change in ΔΔG between FL_4 and $FL_1/WT_1/FL_2$ and FL_2/WT_2 was small compared with the change between tetramers with three or four WT subunits. Overall, the relationship between calculated ΔΔG and the number of WT subunits (i.e., available ICA-binding sites) was intermediate between the linear function predicted for model 2 cooperative subunit interactions and the step function predicted for a fully concerted process requiring the simultaneous cooperation of all four subunits (model 1).

TABLE 2

Summary of effects of ICA on the voltage dependence of activation and inactivation for hERG1 monomers (WT) and tetramers containing zero to four F557L (FL) subunits

Channel type	Control		30 µM ICA		n
	$V_{0.5}$	z	$V_{0.5}$	z	
	mV		*mV*		
$V_{0.5act}$					
WT_4	−30.2 ± 1.0	3.76 ± 0.22	ND[a]	ND[a]	12
FL_1/WT_3	−25.0 ± 0.6	3.76 ± 0.17	−34.5 ± 1.5	4.06 ± 0.39	5
WT_3/FL_1	−26.9 ± 0.9	3.32 ± 0.05	−36.7 ± 1.1	3.57 ± 0.39	4
$FL_1/WT_1/FL_1/WT_1$	−22.7 ± 1.1	2.60 ± 0.05	−29.6 ± 1.6	3.00 ± 0.25	4
FL_2/WT_2	−26.0 ± 1.7	3.04 ± 0.15	−37.1 ± 0.4	3.88 ± 0.48	4
$FL_1/WT_1/FL_2$	−22.0 ± 2.7	3.36 ± 0.18	−19.5 ± 2.9	2.80 ± 0.22	4
FL_4	−16.4 ± 3.3	3.11 ± 0.15	−18.7 ± 1.0	3.60 ± 0.15	3
$V_{0.5inact}$					
WT_4	−54.4 ± 2.6	1.06 ± 0.03	57.8 ± 4.1	1.17 ± 0.05	5
FL_1/WT_3	−45.8 ± 3.0	1.00 ± 0.04	28.5 ± 6.0	0.95 ± 0.13	4
WT_3/FL_1	−57.8 ± 4.4	0.90 ± 0.03	49.9 ± 4.0	1.21 ± 0.03	4
$FL_1/WT_1/FL_1/WT_1$	−51.1 ± 14.3	0.80 ± 0.05	−33.7 ± 16.0	0.56 ± 0.03	4
FL_2/WT_2	−62.7 ± 3.0	0.75 ± 0.05	−22.4 ± 9.3	0.46 ± 0.01	3
$FL_1/WT_1/FL_2$	−79.0 ± 7.8	0.67 ± 0.03	−72.5 ± 7.7	0.61 ± 0.05	4
FL_4	−103.7 ± 2.4	0.65 ± 0.05	−98.8 ± 7.8	0.69 ± 0.04	3

Data are expressed as mean ± SEM (n = number of oocytes).

[a]Not able to measure accurately because tail currents were affected by extracellular K^+ accumulation associated with very large outward currents.

DISCUSSION

Construction of plasmids for expression of concatenated proteins enables the characterization of heterooligomeric protein complexes with precisely defined subunit stoichiometry and geometry. Tandem hERG1 dimers were previously used to characterize binding of hERG1 inhibitors (Imai et al., 2009), but our study is the first to construct and characterize concatenated tetramers for this channel. We took advantage of our previous finding that L646E and F557L mutations nearly abolish the ability of PD and ICA, respectively, to enhance hERG1 currents. Molecular modeling suggests that these mutations interfere with ligand binding, although competitive radiolabeled ligand displacement studies are needed to confirm this prediction and rule out the possibility that the mutations instead disrupt the ability of bound ligand to allosterically alter channel gating.

Concatenated subunits have previously been used to study several voltage-gated K^+ and ligand-gated channels (Isacoff et al., 1990; Yang et al., 1997; Morrill and MacKinnon, 1999; Minier and Sigel, 2004; Sack et al., 2008). Although unusual stoichiometry was observed in some cases (McCormack et al., 1992; Hurst et al., 1995; Sack et al., 2008), concatenated channels can be properly assembled by linking nearly identical subunits (e.g., WT subunits plus subunits containing a single point mutation; Hurst et al., 1992; Sack et al., 2008). However, formation of multimerized concatemers, where two or more tetramers combine to form a functional channel sometimes by exclusion of a mutant subunit, has been described for Kv1.1 (Hurst et al., 1995). In this study, the authors introduced a Pro residue into the S4 segment and a point mutation to alter sensitivity to TEA in one or more subunits of a concatenated tetramer. Analysis of the voltage dependence of activation and block by TEA revealed that Pro-containing subunits were apparently excluded from functional channels, implying that two or more tetramers combined to form a functional channel. Pro substitutions greatly suppressed functional channel expression as currents were only measurable if 100–1,000× more cRNA was injected than was required for expression of WT_4 Kv1.1 channels. In contrast, several features of the tetramer channels we studied suggest that multimerized concatemers were not formed. First, we found that the expression level of concatenated hERG1 tetramers were the same regardless of the number of mutant subunits per tetramer. Second, there was a graded response to drug for tetramers containing variable numbers of F557L or L646E subunits, despite similar biophysical properties measured in the absence of the drug. Third, F557L mutations cause a negative shift in $V_{0.5inact}$ when F557L monomers are expressed in oocytes, and in tetramers containing two or more F557L subunits, there was a progressive negative shift in the $V_{0.5inact}$. Fourth, for both mutations studied (L646E and F557L), there were no significant differences in the biophysical properties of channels where the single mutant subunit was placed in the first or fourth position of the heterotypic tetramer. Moreover, the response to PD or ICA was not altered when the mutant subunit was placed in either the first or last position. We also examined how positioning two WT plus two mutant subunits with like subunits in a diagonal versus an adjacent orientation affected channel properties for all three mutations. The biophysical properties of these channels were similar, whereas the response to drug varied. Although this finding indicates differential effects of drug binding on channel gating, it does not imply that multimerized concatemers were formed.

Positive cooperativity of oligomeric protein function can result when ligand occupancy of one site enhances the ligand affinity of other unbound sites (e.g., O_2 binding to tetrameric hemoglobin [Hill, 1910; Perutz, 1970]) or by cooperative interactions between protomers that can result from ligand binding to multiple sites with the same or similar affinity. The EC_{50} and n_H for PD effects were independent of the number of WT subunits present in a concatenated tetramer, indicating occupancy of one binding site does not lead to enhancement of PD affinity of other sites. Hill coefficients (n_H) >1 derived from fitting the concentration-response relationships for ICA on WT channels indicate positive cooperativity, an effect which could arise from differential affinity of the four available binding sites. For a receptor with four ligand-binding sites, the binding affinity for each successive ligand-bound state would have to increase by an order of magnitude for n_H to reach a value of 4 (Weiss, 1997). Although the efficacy (maximal effect) of ICA varied for concatenated tetramers containing a variable number of available ligand-binding sites, there was little difference between the EC_{50} or n_H values for WT_4 and $FL_1/WT_1/FL_2$ channels. Thus, we conclude that the agonist effects of PD and ICA on hERG1

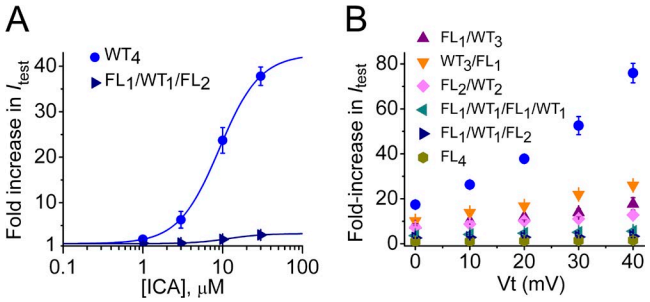

Figure 8. Concentration- and voltage-dependent effects of ICA on I_{test}. (A) Concentration-dependent increase in I_{test} measured at 20 mV by ICA for WT_4 and $FL_1/WT_1/FL_2$ hERG1 concatenated channels. Data were fitted with a logistic equation (smooth curves). For WT_4 channels: EC_{50} = 9.1 µM, n_H = 1.7 (n = 6–9); for $FL_1/WT_1/FL_2$ channels: EC_{50} = 11.8 µM, n_H = 2.0 (n = 6–10). (B) Fold increase in I_{test} by 30 µM ICA as a function of V_t (n = 3–8). Data are expressed as mean ± SEM (n = number of oocytes).

derive from cooperative subunit interactions and not from positive cooperativity of drug binding to multiple sites on a single channel.

Similar to many oligomeric enzymes (Monod et al., 1965), multimeric ion channels have the capacity to mediate homotropic cooperative interactions. For example, potentiation of pentameric α7 nicotinic receptors by the type II–positive allosteric modulator PNU-120596, caused by slowing of channel desensitization, is mediated by highly cooperative subunit interactions. At least four and perhaps five of the available PNU-120596–binding sites must be occupied to achieve maximal channel activation (daCosta and Sine, 2013). In contrast, activation of the same receptors by the native ligand acetylcholine involves independent subunit interactions. Occupancy of only one of the five available binding sites by acetylcholine is sufficient to fully activate α7 nicotinic receptors (Andersen et al., 2013). Thus, subunit interaction can vary widely depending on the ligand used to interrogate channel function. We examined the effects of two hERG1 agonists with different mechanisms of action but with overlapping binding sites. Both PD and ICA bind to a hydrophobic pocket located between two adjacent hERG1 subunits, and thus, a homotetrameric channel has four identical binding sites. The ability of PD to increase current magnitude, quantified by ΔG ($-RTlnK_{eq}$) was enhanced in direct proportion to the WT/L646E subunit ratio, indicating full cooperativity among subunits. A similar mode of interaction between WT and mutant subunits in concatenated tetramers was previously reported for the activation and block by TEA of Kv1.1 channels (Hurst et al., 1992). The $V_{0.5}$ for activation of Kv1.1 was shifted to more positive potentials as a linear function of the number of subunits containing a L305I mutation, and the free energy of binding of TEA was linearly related to the number of subunits containing Tyr379 (a residue in the outer pore which mediates high-affinity TEA binding). These results

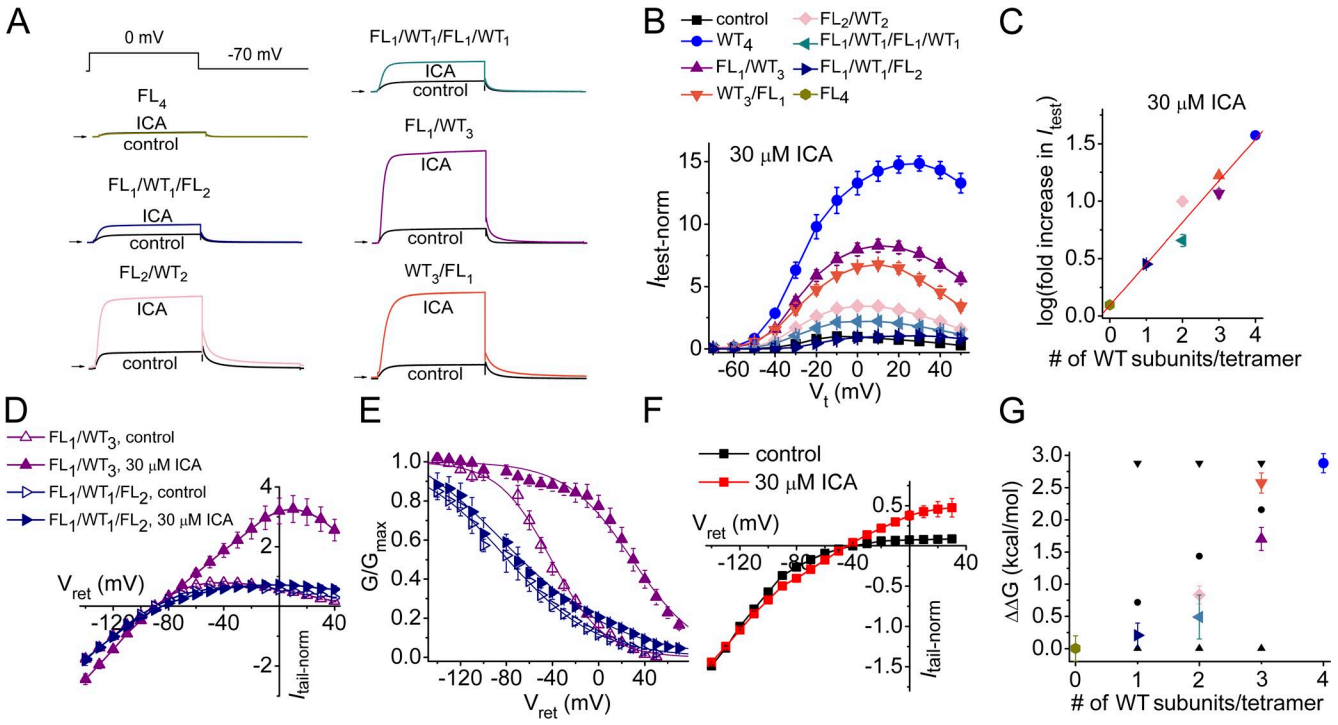

Figure 9. Attenuation of hERG1 inactivation by ICA exhibits positive cooperativity. (A) Representative current traces under control conditions and after 10 μM ICA for tetramers containing the indicated number and orientation of WT and F557L subunits. (B) Normalized I_{test}-V_t relationships for concatenated tetramers measured in the presence of 30 μM ICA (n = 4–10). Currents were normalized to the peak I_{test} under control conditions for each channel type. Symbol legends refer to data plotted in B, C, and G. (C) Correlation between log fold increase in I_{test} at 20 mV induced by 30 μM ICA and the number of WT subunits (i.e., number of functional ICA binding sites) in a concatenated tetramer. Data were fitted with a linear function: y = 0.36x + 0.1 (R^2 = 0.94). (D) Fully activated I_{tail}-V_{ret} relationship for FL_1/WT_3 and $FL_1/WT_1/FL_2$ tetramers before and after 30 μM ICA (n = 4). Currents were normalized to control I_{tail} at −120 mV. (E) Voltage dependence of inactivation for FL_1/WT_3 and $FL_1/WT_1/FL_2$ tetramers before and after 30 μM ICA (n = 4). $V_{0.5inact}$ and z values are presented in Table 2. (F) Effect of 30 μM ICA on the fully activated I_{tail}-V_{ret} relationships for WT_4 channel currents recorded from oocytes bathed in a solution containing 20 mM KCl (n = 4). Data were normalized to I_{tail} measured at −120 mV under control conditions. (G) Plot of calculated energy values, $\Delta\Delta G = \left|zFV_{0.5inact}(30\mu M\ ICA) - zFV_{0.5inact}(control)\right|$, versus number of WT subunits contained in a concatenated tetramer compared with the relationships predicted for independent subunit transitions (▼) and cooperative subunit interactions, models 1 (▲) and 2 (●). Data are expressed as mean ± SEM (n = number of oocytes). Standard errors in $zFV_{0.5inact}$ were calculated as described previously (Yifrach and MacKinnon, 2002).

indicate that each of the four subunits in a WT channel contributes equally to the formation of the TEA-binding site and to the voltage dependence of channel activation (Hurst et al., 1992). Analysis of the rate and voltage dependence of activation of Shaw/Shaker heterodimer channels also indicates cooperative subunit interactions, and the total energy associated with channel opening is approximated by assuming that ΔG for each subunit type was additive (Smith-Maxwell et al., 1998). A full complement of concatenated tetramers incorporating WT subunits or mutant subunits (containing G466P to disrupt the S6 gating hinge) was also used to characterize subunit cooperativity in the activation of Shaker channels (Zandany et al., 2008). It was found that a single G466P subunit in any position of the tetramer caused the same negative shift in the voltage dependence of activation ($\Delta\Delta G \cong 6$ kcal/mol), as was achieved with all other heterotypic tetramers or the tetramer containing all mutant subunits. Thus, in contrast to other S4 segment mutations used to probe for subunit cooperativity (Hurst et al., 1992; Smith-Maxwell et al., 1998), a mutation that directly disrupts the gating hinge (G466P) provides a direct demonstration that activation of Kv channels requires all-or-none (i.e., fully concerted) participation of subunits to open the activation gate.

Subunit cooperativity has also been described for C-type inactivation of Kv channels (Ogielska et al., 1995; Panyi et al., 1995), a gating process which prevents K^+ flux, either by constriction (Yellen et al., 1994) or dilation (Hoshi and Armstrong, 2013) of the narrowest region of the channel pore formed by the selectivity filter. Although C-type inactivation is very slow and voltage independent in Shaker (Kv1) channels (Hoshi et al., 1991), it is extremely fast and voltage dependent in hERG1 (Kv11.1) channels (Smith et al., 1996; Spector et al., 1996). C-type inactivation of hERG1 can also be disrupted by mutation of specific residues in or near the selectivity filter (e.g., G628C/S631C; Smith et al., 1996) or pore helix (e.g., S620T; Ficker et al., 1998). ICA-mediated shifts in the voltage dependence of C-type inactivation of hERG1 also involve subunit cooperativity. $\Delta\Delta G$ calculated from the differences between steady-state inactivation curves before and after ICA was a nonlinear function of the number of WT subunits (i.e., available ICA binding sites), indicating a more complex mode of cooperativity than reported for C-type inactivation of Kv1.3 channels probed with a point mutation (A413V) that accelerates inactivation (Panyi et al., 1995). Each A413V-containing subunit was shown to contribute equally ($\sim$0.6 kcal/mol) to the activation free energy for transitions between O and I states.

In summary, construction and characterization of concatenated heterotetrameric channels have revealed the stoichiometry of allosteric alteration of channel gating by hERG1 agonists. Increased P_o by PD and inhibition of C-type inactivation by ICA involve subunit cooperativity, and occupancy of all four available binding sites is required for maximal effect of both compounds. A detailed understanding of how these and other compounds allosterically modify selectivity filter gating should aid rational design of drugs that can be used to prevent arrhythmias associated with inherited and acquired long QT syndrome.

We thank Kirk Thomas and Vivek Garg for valuable discussions.

This work was supported by National Institutes of Health/National Heart, Lung, and Blood Institute grant R01 HL055236 (to M.C. Sanguinetti).

The authors declare no competing financial interests.

Sharona E. Gordon served as editor.

Submitted: 28 May 2013
Accepted: 14 February 2014

REFERENCES

Abbruzzese, J., F.B. Sachse, M. Tristani-Firouzi, and M.C. Sanguinetti. 2010. Modification of hERG1 channel gating by Cd^{2+}. *J. Gen. Physiol.* 136:203–224. http://dx.doi.org/10.1085/jgp.201010450

Andersen, N., J. Corradi, S.M. Sine, and C. Bouzat. 2013. Stoichiometry for activation of neuronal α7 nicotinic receptors. *Proc. Natl. Acad. Sci. USA.* 110:20819–20824. http://dx.doi.org/10.1073/pnas.1315775110

Bianchi, L., B. Wible, A. Arcangeli, M. Taglialatela, F. Morra, P. Castaldo, O. Crociani, B. Rosati, L. Faravelli, M. Olivotto, and E. Wanke. 1998. herg encodes a K^+ current highly conserved in tumors of different histogenesis: A selective advantage for cancer cells? *Cancer Res.* 58:815–822.

Curran, M.E., I. Splawski, K.W. Timothy, G.M. Vincent, E.D. Green, and M.T. Keating. 1995. A molecular basis for cardiac arrhythmia: *HERG* mutations cause long QT syndrome. *Cell.* 80:795–803. http://dx.doi.org/10.1016/0092-8674(95)90358-5

daCosta, C.J., and S.M. Sine. 2013. Stoichiometry for drug potentiation of a pentameric ion channel. *Proc. Natl. Acad. Sci. USA.* 110:6595–6600. http://dx.doi.org/10.1073/pnas.1301909110

Fenichel, R.R., M. Malik, C. Antzelevitch, M. Sanguinetti, D.M. Roden, S.G. Priori, J.N. Ruskin, R.J. Lipicky, and L.R. Cantilena; Independent Academic Task Force. 2004. Drug-induced torsades de pointes and implications for drug development. *J. Cardiovasc. Electrophysiol.* 15:475–495. http://dx.doi.org/10.1046/j.1540-8167.2004.03534.x

Ficker, E., W. Jarolimek, J. Kiehn, A. Baumann, and A.M. Brown. 1998. Molecular determinants of dofetilide block of HERG K^+ channels. *Circ. Res.* 82:386–395. http://dx.doi.org/10.1161/01.RES.82.3.386

Garg, V., A. Stary-Weinzinger, F. Sachse, and M.C. Sanguinetti. 2011. Molecular determinants for activation of human *ether-à-go-go-related* gene 1 potassium channels by 3-nitro-*N*-(4-phenoxyphenyl) benzamide. *Mol. Pharmacol.* 80:630–637. http://dx.doi.org/10.1124/mol.111.073809

Gerlach, A.C., S.J. Stoehr, and N.A. Castle. 2010. Pharmacological removal of human *ether-à-go-go*-related gene potassium channel inactivation by 3-nitro-*N*-(4-phenoxyphenyl) benzamide (ICA-105574). *Mol. Pharmacol.* 77:58–68. http://dx.doi.org/10.1124/mol.109.059543

Goldin, A.L. 1991. Expression of ion channels by injection of mRNA into *Xenopus* oocytes. *Methods Cell Biol.* 36:487–509. http://dx.doi.org/10.1016/S0091-679X(08)60293-9

Hansen, R.S., T.G. Diness, T. Christ, J. Demnitz, U. Ravens, S.P. Olesen, and M. Grunnet. 2006. Activation of human *ether-a-go-go*-related

gene potassium channels by the diphenylurea 1,3-bis-(2-hydroxy-5-trifluoromethyl-phenyl)-urea (NS1643). *Mol. Pharmacol.* 69:266–277.

Hill, A.V. 1910. The possible effects of the aggregation of the molecules of haemoglobin on its dissociation curves. *J. Physiol.* 40:iv–vii.

Hoshi, T., and C.M. Armstrong. 2013. C-type inactivation of voltage-gated K^+ channels: Pore constriction or dilation? *J. Gen. Physiol.* 141:151–160. http://dx.doi.org/10.1085/jgp.201210888

Hoshi, T., W.N. Zagotta, and R.W. Aldrich. 1991. Two types of inactivation in *Shaker* K^+ channels: Effects of alterations in the carboxy-terminal region. *Neuron.* 7:547–556. http://dx.doi.org/10.1016/0896-6273(91)90367-9

Huffaker, S.J., J. Chen, K.K. Nicodemus, F. Sambataro, F. Yang, V. Mattay, B.K. Lipska, T.M. Hyde, J. Song, D. Rujescu, et al. 2009. A primate-specific, brain isoform of KCNH2 affects cortical physiology, cognition, neuronal repolarization and risk of schizophrenia. *Nat. Med.* 15:509–518. http://dx.doi.org/10.1038/nm.1962

Hurst, R.S., M.P. Kavanaugh, J. Yakel, J.P. Adelman, and R.A. North. 1992. Cooperative interactions among subunits of a voltage-dependent potassium channel. Evidence from expression of concatenated cDNAs. *J. Biol. Chem.* 267:23742–23745.

Hurst, R.S., R.A. North, and J.P. Adelman. 1995. Potassium channel assembly from concatenated subunits: Effects of proline substitutions in S4 segments. *Receptors Channels.* 3:263–272.

Imai, Y.N., S. Ryu, and S. Oiki. 2009. Docking model of drug binding to the human *ether-à-go-go* potassium channel guided by tandem dimer mutant patch-clamp data: A synergic approach. *J. Med. Chem.* 52:1630–1638. http://dx.doi.org/10.1021/jm801236n

Isacoff, E.Y., Y.N. Jan, and L.Y. Jan. 1990. Evidence for the formation of heteromultimeric potassium channels in *Xenopus* oocytes. *Nature.* 345:530–534. http://dx.doi.org/10.1038/345530a0

Iyer, V., R. Mazhari, and R.L. Winslow. 2004. A computational model of the human left-ventricular epicardial myocyte. *Biophys. J.* 87:1507–1525. http://dx.doi.org/10.1529/biophysj.104.043299

Kang, J., X.L. Chen, H. Wang, J. Ji, H. Cheng, J. Incardona, W. Reynolds, F. Viviani, M. Tabart, and D. Rampe. 2005. Discovery of a small molecule activator of the human *ether-a-go-go*-related gene (HERG) cardiac K^+ channel. *Mol. Pharmacol.* 67:827–836. http://dx.doi.org/10.1124/mol.104.006577

Keating, M.T., and M.C. Sanguinetti. 2001. Molecular and cellular mechanisms of cardiac arrhythmias. *Cell.* 104:569–580. http://dx.doi.org/10.1016/S0092-8674(01)00243-4

MacKinnon, R. 1991. Determination of the subunit stoichiometry of a voltage-activated potassium channel. *Nature.* 350:232–235. http://dx.doi.org/10.1038/350232a0

MacKinnon, R., R.W. Aldrich, and A.W. Lee. 1993. Functional stoichiometry of Shaker potassium channel inactivation. *Science.* 262:757–759. http://dx.doi.org/10.1126/science.7694359

McCormack, K., L. Lin, L.E. Iverson, M.A. Tanouye, and F.J. Sigworth. 1992. Tandem linkage of Shaker K^+ channel subunits does not ensure the stoichiometry of expressed channels. *Biophys. J.* 63:1406–1411. http://dx.doi.org/10.1016/S0006-3495(92)81703-4

Minier, F., and E. Sigel. 2004. Techniques: Use of concatenated subunits for the study of ligand-gated ion channels. *Trends Pharmacol. Sci.* 25:499–503. http://dx.doi.org/10.1016/j.tips.2004.07.005

Monod, J., J. Wyman, and J.P. Changeux. 1965. On the nature of allosteric transitions: A plausible model. *J. Mol. Biol.* 12:88–118. http://dx.doi.org/10.1016/S0022-2836(65)80285-6

Morrill, J.A., and R. MacKinnon. 1999. Isolation of a single carboxyl-carboxylate proton binding site in the pore of a cyclic nucleotide–gated channel. *J. Gen. Physiol.* 114:71–84. http://dx.doi.org/10.1085/jgp.114.1.71

Ogielska, E.M., W.N. Zagotta, T. Hoshi, S.H. Heinemann, J. Haab, and R.W. Aldrich. 1995. Cooperative subunit interactions in C-type inactivation of K channels. *Biophys. J.* 69:2449–2457. http://dx.doi.org/10.1016/S0006-3495(95)80114-1

Panyi, G., Z. Sheng, and C. Deutsch. 1995. C-type inactivation of a voltage-gated K^+ channel occurs by a cooperative mechanism. *Biophys. J.* 69:896–903. http://dx.doi.org/10.1016/S0006-3495(95)79963-5

Perry, M., F.B. Sachse, and M.C. Sanguinetti. 2007. Structural basis of action for a human *ether-a-go-go*-related gene 1 potassium channel activator. *Proc. Natl. Acad. Sci. USA.* 104:13827–13832. http://dx.doi.org/10.1073/pnas.0703934104

Perry, M., F.B. Sachse, J. Abbruzzese, and M.C. Sanguinetti. 2009. PD-118057 contacts the pore helix of hERG1 channels to attenuate inactivation and enhance K^+ conductance. *Proc. Natl. Acad. Sci. USA.* 106:20075–20080. http://dx.doi.org/10.1073/pnas.0906597106

Perutz, M.F. 1970. Stereochemistry of cooperative effects in haemoglobin. *Nature.* 228:726–734. http://dx.doi.org/10.1038/228726a0

Sack, J.T., O. Shamotienko, and J.O. Dolly. 2008. How to validate a heteromeric ion channel drug target: Assessing proper expression of concatenated subunits. *J. Gen. Physiol.* 131:415–420. http://dx.doi.org/10.1085/jgp.200709939

Sanguinetti, M.C., and N.K. Jurkiewicz. 1990. Two components of cardiac delayed rectifier K^+ current. Differential sensitivity to block by class III antiarrhythmic agents. *J. Gen. Physiol.* 96:195–215. http://dx.doi.org/10.1085/jgp.96.1.195

Sanguinetti, M.C., C. Jiang, M.E. Curran, and M.T. Keating. 1995. A mechanistic link between an inherited and an acquired cardiac arrhythmia: *HERG* encodes the I_{Kr} potassium channel. *Cell.* 81:299–307. http://dx.doi.org/10.1016/0092-8674(95)90340-2

Schreibmayer, W., H.A. Lester, and N. Dascal. 1994. Voltage clamping of *Xenopus laevis* oocytes utilizing agarose-cushion electrodes. *Pflugers Arch.* 426:453–458. http://dx.doi.org/10.1007/BF00388310

Sigworth, F.J. 1994. Voltage gating of ion channels. *Q. Rev. Biophys.* 27:1–40. http://dx.doi.org/10.1017/S0033583500002894

Smith, P.L., T. Baukrowitz, and G. Yellen. 1996. The inward rectification mechanism of the HERG cardiac potassium channel. *Nature.* 379:833–836. http://dx.doi.org/10.1038/379833a0

Smith-Maxwell, C.J., J.L. Ledwell, and R.W. Aldrich. 1998. Role of the S4 in cooperativity of voltage-dependent potassium channel activation. *J. Gen. Physiol.* 111:399–420. http://dx.doi.org/10.1085/jgp.111.3.399

Spector, P.S., M.E. Curran, A. Zou, M.T. Keating, and M.C. Sanguinetti. 1996. Fast inactivation causes rectification of the I_{Kr} channel. *J. Gen. Physiol.* 107:611–619. http://dx.doi.org/10.1085/jgp.107.5.611

Stühmer, W. 1992. Electrophysiological recording from *Xenopus* oocytes. *Methods Enzymol.* 207:319–339. http://dx.doi.org/10.1016/0076-6879(92)07021-F

Trudeau, M.C., J.W. Warmke, B. Ganetzky, and G.A. Robertson. 1995. HERG, a human inward rectifier in the voltage-gated potassium channel family. *Science.* 269:92–95. http://dx.doi.org/10.1126/science.7604285

Tytgat, J., and P. Hess. 1992. Evidence for cooperative interactions in potassium channel gating. *Nature.* 359:420–423. http://dx.doi.org/10.1038/359420a0

Weiss, J.N. 1997. The Hill equation revisited: Uses and misuses. *FASEB J.* 11:835–841.

Yang, Y., Y. Yan, and F.J. Sigworth. 1997. How does the W434F mutation block current in *Shaker* potassium channels? *J. Gen. Physiol.* 109:779–789. http://dx.doi.org/10.1085/jgp.109.6.779

Yellen, G., D. Sodickson, T.-Y. Chen, and M.E. Jurman. 1994. An engineered cysteine in the external mouth of a K^+ channel allows inactivation to be modulated by metal binding. *Biophys. J.* 66:1068–1075. http://dx.doi.org/10.1016/S0006-3495(94)80888-4

Yifrach, O., and R. MacKinnon. 2002. Energetics of pore opening in a voltage-gated K^+ channel. *Cell.* 111:231–239. http://dx.doi.org/10.1016/S0092-8674(02)01013-9

Zagotta, W.N., T. Hoshi, and R.W. Aldrich. 1994. Shaker potassium channel gating. III: Evaluation of kinetic models for activation. *J. Gen. Physiol.* 103:321–362. http://dx.doi.org/10.1085/jgp.103.2.321

Zamorano-León, J.J., R. Yañez, G. Jaime, P. Rodriguez-Sierra, L. Calatrava-Ledrado, R.R. Alvarez-Granada, P.J. Mateos-Cáceres, C. Macaya, and A.J. López-Farré. 2012. KCNH2 gene mutation: a potential link between epilepsy and long QT-2 syndrome. *J. Neurogenet.* 26:382–386. http://dx.doi.org/10.3109/01677063.2012.674993

Zandany, N., M. Ovadia, I. Orr, and O. Yifrach. 2008. Direct analysis of cooperativity in multisubunit allosteric proteins. *Proc. Natl. Acad. Sci. USA.* 105:11697–11702. http://dx.doi.org/10.1073/pnas.0804104105

Zou, A., Q.P. Xu, and M.C. Sanguinetti. 1998. A mutation in the pore region of HERG K^+ channels expressed in *Xenopus* oocytes reduces rectification by shifting the voltage dependence of inactivation. *J. Physiol.* 509:129–137. http://dx.doi.org/10.1111/j.1469-7793.1998.129bo.x

Zhou, J., C.E. Augelli-Szafran, J.A. Bradley, X. Chen, B.J. Koci, W.A. Volberg, Z. Sun, and J.S. Cordes. 2005. Novel potent human *ether-a-go-go*-related gene (hERG) potassium channel enhancers and their in vitro antiarrhythmic activity. *Mol. Pharmacol.* 68:876–884.

Wu et al., http://www.jgp.org/cgi/content/full/jgp.201311038/DC1

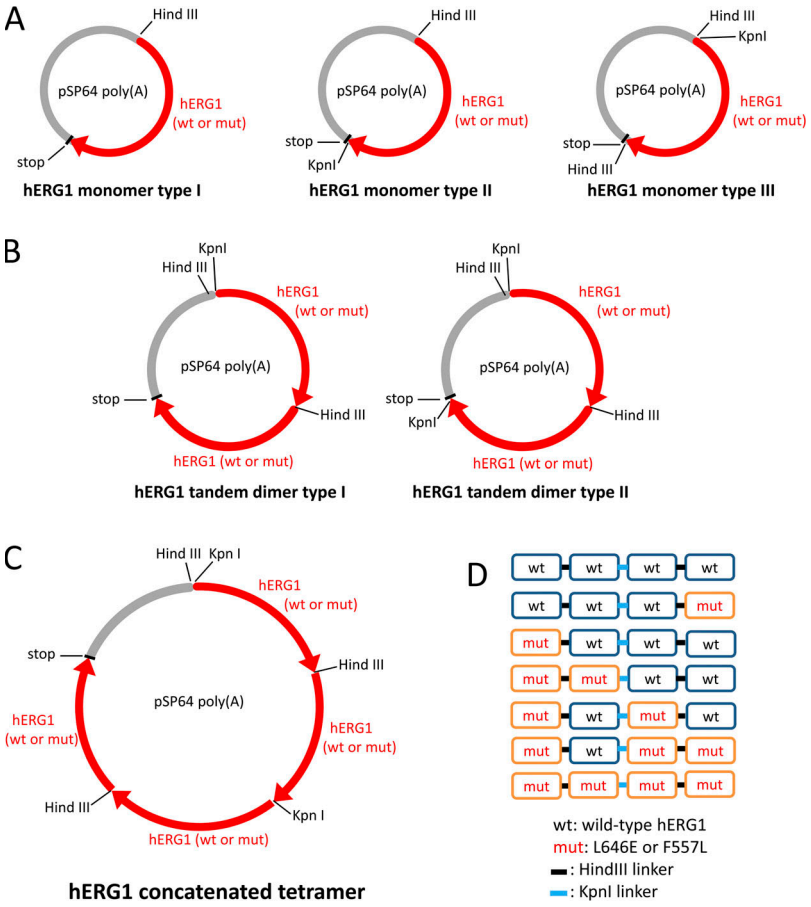

Figure S1. Schematic plasmid maps for *KCNH2* monomers, tandem dimers, and concatenated tetramers with different patterns of restriction enzyme sites. (A) Plasmid maps for type I–III *KCNH2* monomers with HindIII sites and KpnI sites. (B) Plasmid maps for type I and II *KCNH2* tandem dimers with either one or two KpnI sites. Type I tandem dimers were linked by HindIII between type I and III monomers, whereas type II tandem dimers were concatenated by HindIII between type II and III monomers. (C) Plasmid map for concatenated *KCNH2* tetramer. The final concatenated *KCNH2* tetramers were linked by KpnI between type I and II tandem dimers. (D) Generalized linear diagrams for the WT_4 and the six different concatenated *KCNH2* tetramers containing one or more mutant subunit.

Table S1

Initial and calculated values of rate constant parameters for modeling effects of PD

Parameter	Symbol	Initial values	WT_4		Unit
			Control	30 μM PD	
Closed-closed transitions	α_{CC}	184.500	56.194	56.194	s^{-1}
	$z_{\alpha CC}$	0.3200	0.717	0.717	
	β_{CC}	1,342.500	32.293	32.293	s^{-1}
	$z_{\beta CC}$	0.3180	0.680	0.680	
Closed-open transitions	α_{C0}	24.000	89.911	205.162	s^{-1}
	β_{C0}	37.000	2.773	2.427	s^{-1}
Open-inactivated transitions	α_{0I}	500.000	947.927	227.232	s^{-1}
	$z_{\alpha OI}$	0.500	0.871	0.785	
	β_{0I}	61.700	52.624	28.505	s^{-1}
	$z_{\beta OI}$	0.500	0.136	0.417	

Table S2

Calculated values of rate constant parameters for modeling effects of ICA

Parameter	WT_4	Unit
	30 μM ICA	
α_{CC}	65.002	s^{-1}
$z_{\alpha CC}$	1.099	
β_{CC}	26.366	s^{-1}
$z_{\beta CC}$	0.006	
α_{C0}	11.762	s^{-1}
β_{C0}	0.576	s^{-1}
α_{0I}	1.137	s^{-1}
$z_{\alpha OI}$	0.441	
β_{0I}	3.567	s^{-1}
$z_{\beta OI}$	0.070	

Calculated parameter values for WT_4 control in Table S1 were applied as initial values for the parameter optimization.

Table S3

Features for PD model fitting and their fit errors

Feature	Weighting factor	E_i: WT_4	
		Control	30 μM PD
$I_{test\text{-}max}$	1	0.143	0.271
$I_{test\text{-}end}$	1	0.153	0.153
$\tau_{test\text{-}slow}$	1.5	0.790	0.582
$\tau_{test\text{-}fast}$	1	0.319	0.383
$I_{tail\text{-}max}$	3	0.247	0.190
$I_{tail\text{-}end}$	0.5	0.326	0.314
$\tau_{tail\text{-}slow}$	1.5	0.191	0.022
$\tau_{tail\text{-}fast}$	1	0.170	0.120
$I_{tail}V_{ret}$	2	0.426	0.311
$1-\mathrm{Max}\sum_j C_j$	20	0.002	0.004
O_{Max} − Max O	4	0.102	0.014
1 − Max(C_4 + O + I)	1	0.000	0.000

$E_i = \left\| f_{m,i} - f_{e,i} \right\|_2 / \left\| f_{e,i} \right\|_2$. $I_{test\text{-}max}$, maximal normalized current during test pulse; $I_{test\text{-}end}$, normalized current at the end of test pulse; $\tau_{test\text{-}slow}$, slow time constant from biexponential fit of current during test pulse; $\tau_{test\text{-}fast}$, fast time constant from biexponential fit of current during test pulse; $I_{tail\text{-}max}$, maximal normalized tail current; $I_{tail\text{-}end}$, normalized current at the end of −70-mV pulse; $\tau_{test\text{-}slow}$, slow time constant from biexponential fit of tail current; $\tau_{test\text{-}fast}$, fast time constant from biexponential fit of tail current; $I_{tail}V_{ret}$, fully activated I-V. Weighting factors were applied to emphasize or deemphasize features.

Table S4

Features for ICA model fitting and their fit errors E_i

Feature	Weighting factor	E_i: WT_4
		30 μM ICA
$I_{test\text{-}max}$	4	0.208
$I_{test\text{-}end}$	4	0.129
$\tau_{test\text{-}slow}$	2	0.591
$\tau_{test\text{-}fast}$	1	0.179
$I_{tail\text{-}max}$	0.5	0.425
$I_{tail\text{-}end}$	0.5	0.114
$\tau_{tail\text{-}slow}$	1	0.050
$I_{tail}V_{ret}$	2	0.373
$1-\mathrm{Max}\sum_j C_j$	20	0.056
O_{Max} − Max O	4	0.183
1 − Max(C_4 + O + I)	1	0.001